Magnetic Resonance in Medicine 54:486–490 (2005)

Diffusion Tensor Imaging Using Partial Fourier STEAM MRI with Projection onto Convex Subsets Reconstruction

Susanne Rieseberg, Klaus-Dietmar Merboldt, Matthias Küntzel, and Jens Frahm*

Diffusion-weighted single-shot STEAM MRI allows for diffusion mapping of the human brain without sensitivity to resonance offset effects. In order to compensate for its inherently lower SNR and speed than echo-planar imaging, this work describes the use of partial Fourier encoding in combination with image reconstruction by the projection onto convex subsets algorithm. The method overcomes phase distortions in diffusion-weighted partial Fourier acquisitions that disturb the conjugate complex symmetry of *k*-space and preclude the use of respective reconstruction techniques. In comparison with full Fourier encoding and a static flip angle for the STEAM readout pulses, experimental results at 2.9 T demonstrate a gain in relative SNR per unit time by 20% for 5/8 phase encoding with optimized variable flip angles. Simultaneously, the imaging time is reduced from about 670 ms (80 echoes) to 440 ms (50 echoes). Current implementations at 2 × 2 mm^2 in-plane resolution comprise a protocol for clinical anisotropy studies (12 diffusion-encoding gradient directions at 1000 s mm^{-2}) covering 18 sections of 4-mm thickness within a measurement time of 8.5 min (5 averages) and a version optimized for fiber tracking using 24 gradient directions and 38 sections of 2-mm thickness yielding a measurement time of 29.5 min (4 averages). Magn Reson Med 54:486–490, 2005. © 2005 Wiley-Liss, Inc.

Key words: human brain; diffusion tensor imaging; STEAM MRI; POCS; partial Fourier

The increasing availability and use of diffusion-weighted (DW) single-shot echo-planar imaging (EPI) in basic and clinical neuroscience renders the accompanying signal void and geometric distortions due to magnetic susceptibility differences a problem of utmost importance. In fact, a definite solution to the resonance offset problem in diffusion tensor imaging (DTI) must be considered mandatory for its integration into any clinical decision making. Proposals to improve EPI acquisitions range from postacquisition corrections to a reduction of the echo train length by multishot sequences or parallel imaging. In fact, these latter approaches effectively reduce the degree of T_2^* weighting and ameliorate corresponding image artifacts. On the other hand, higher field strengths such as 3 T or above at least partly counterbalance this improvement by a pronounced decrease of white matter T_2 (and T_2^*) relaxation times.

In contrast, MRI sequences with radiofrequency-refocused echoes exhibit no sensitivity to magnetic field inhomogeneities and susceptibility differences. In an earlier contribution we described DW single-shot stimulated echo acquisition mode (STEAM) MRI as a means to obtain distortion-free diffusion tensor maps of the human brain (1). The prize to be paid is a longer measuring time and lower SNR than obtainable with EPI. Subsequently, it could be shown that (non-DW) single-shot STEAM MRI may be improved by the use of conventional half Fourier (HF) phase encoding (2). The correspondingly shorter train of stimulated echoes reduces the image acquisition time and simultaneously improves the SNR. This is because the possible flip angle increase for the STEAM readout pulses overcompensates the SNR reduction due to a lower number of stimulated echoes.

The purpose of this contribution is to extend our previous work on DW single-shot STEAM MRI to the general case of partial Fourier (PF) imaging (3). Unfortunately, a straightforward reconstruction of DW PF images using the conjugate complex symmetry of *k*-space is precluded by the fact that the diffusion gradients enhance the spatially inhomogeneous phase distribution observed in vivo to such a degree that respective reconstructions fail to achieve undistorted images. Here, it is demonstrated that the expected increase in SNR and speed of PF versions can be realized if the images are reconstructed with use of the projection onto convex subsets (POCS) algorithm (4,5). The gain in performance is demonstrated for applications to human brain.

MATERIALS AND METHODS

All studies were conducted at 2.9 T (Siemens Magnetom Trio, Erlangen, Germany) using 40 mT m^{-1} gradients with a maximum slew rate of 200 mT m^{-1} ms^{-1}. Images were acquired with a receive-only eight-channel phased-array head coil (Siemens, Erlangen, Germany) and a body coil for RF transmission. Written informed consent was obtained from all subjects prior to the examination. Anatomic imaging was based on T_1-weighted 3D FLASH MRI sequences (TR/TE = 11/4.9 ms, flip angle 15°).

Diffusion tensor analyses were performed with the use of software developed in-house. Diffusion data acquired at 2 mm isotropic resolution were linearly interpolated to 1 mm isotropic resolution and subjected to a 3D Gaussian filter (σ = 1 voxel). The subsequent calculation of the diffusion tensor employed a weighted linear least-squares algorithm.

Diffusion-Weighted Single-Shot STEAM MRI

Figure 1 depicts a DW version of a single-shot STEAM MRI sequence with middle interval TM and low-flip angle readout pulses α that refocus a train of stimulated echoes (STE) with echo time TE_{STE} and repetition time TR. For diffusion encoding, the initial 90° pulse of the single-shot STEAM MRI sequence (6) is replaced by a (virtual) spin-echo signal

Biomedizinische NMR Forschungs GmbH am Max-Planck-Institut für biophysikalische Chemie, Göttingen, Germany.

*Correspondence to: J. Frahm, Biomedizinische NMR Forschungs GmbH, 37070 Göttingen, Germany. E-mail: jfrahm@gwdg.de

Received 3 September 2004; revised 19 January 2005; accepted 11 March 2005.

DOI 10.1002/mrm.20572
Published online in Wiley InterScience (www.interscience.wiley.com).

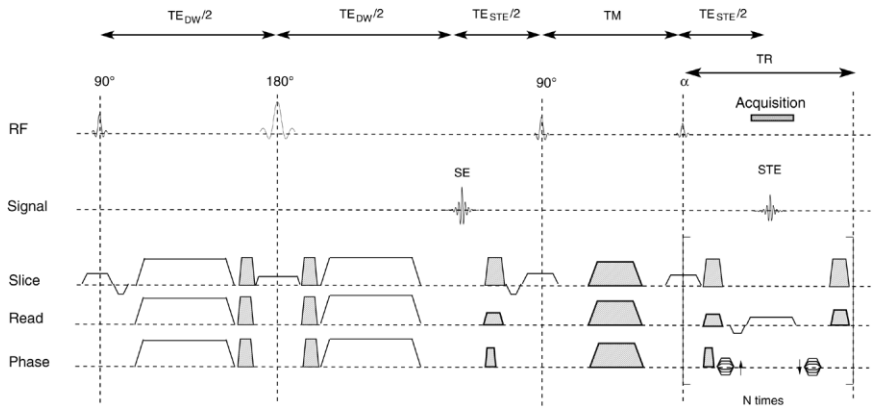

FIG. 1. Schematic sequence diagram for diffusion-weighted single-shot STEAM MRI with spoiler moments (shaded) separated from the imaging gradients. For details see text.

(SE), which results from the application of a single 90–180° spin-echo interval. Specific spoiler moments (shaded areas in Fig. 1) are required to dephase magnetizations that do not belong to the coherence pathway of the stimulated echo but nevertheless reach zero phase during the readout interval. Respective moments were applied along all three logical directions of the imaging gradients comprising balanced spoiler gradients in the $TE_{STE}/2$-intervals and spoiler gradients during TM. After data acquisition, residual magnetizations during TR are spoiled by gradients applied along the slice and readout direction. Because unnecessarily high slew rates may lead to physiologic nerve stimulation or cause eddy currents and respective image artifacts, the spoiler gradients in readout direction were reduced as far as possible while maintaining a strong spoiler moment along the slice selection direction. While the schematic representation shown in Fig. 1 depicts all spoiler moments as separate gradients from the imaging gradients, practical implementations merge respective moments where possible.

For applications to human brain, DW single-shot STEAM MRI was performed at 2×2 mm^2 in-plane resolution using a rectangular 160×256 mm^2 field of view in conjunction with an acquisition matrix of 80×128, 50×128, and 44×128 for full Fourier (FF), 5/8 PF, and HF encoding, respectively. The bandwidth of the acquisition was optimized for SNR while avoiding spatial blurring due to the echo decay. This takes into account that the strength of a particular STE signal is determined by the flip angle of its readout pulse, the availability of residual longitudinal magnetization left over from preceding readout pulses, and the absolute length of the echo train, that is the amount of T_1 relaxation on the initially prepared magnetization during the effective TM (1). Thus, using $SNR \sim \sin\alpha / \sqrt{bw}$ and $TR = 1/bw + T_{res}$ with bw the receiver bandwidth (or acquisition period 1/bw) and T_{res} the residual time required for gradient switching during TR, the SNR may be described as a function of bandwidth (3). For white matter at 3 T ($T_1 \approx 800$ ms) the analysis results in a value of about 180 Hz/pixel (1/bw = 5.5 ms) with TR values of 7.3–7.8 ms for section thicknesses of 2–4 mm. Thus, in comparison with previous implementations at 2.0 T (1,2), the prolonged T_1 relaxation times allowed for a reduction of the optimal bandwidth.

Diffusion encoding employed b values of 0 and 1000 s mm^{-2} with a diffusion time of 28.7 ms (gradient duration 17.4 ms). The corresponding echo time TE_{DW} was made as short as possible to minimize T_2 relaxation losses and long enough to allow for a sufficient diffusion time and a suitable set of diffusion gradients. Here, the echo time was kept at 50.1 ms. Complementing the acquisition of one non-DW image, diffusion encoding was accomplished with use of either 12 or 24 gradient directions, that is two sets of either 6 or 12 gradients with opposite sign. In either case, the arrangement of gradient orientations followed the icosahedron scheme (7), which has been shown to possess an advantageously low and rotationally invariant condition number (8). This finding was consistent with own experimental observations (3).

Practical implementations focused on two different protocols: (i) 18 sections with 4-mm thickness required a multislice repetition time of 7.5 s, which in conjunction with 12 gradient directions (corresponding to the acquisition of 13 images) resulted in a total measuring time of 1.6 min, and (ii) 38 sections with 2-mm thickness and a corresponding multislice repetition time of 17.7 s yielded a minimum measuring time of 7.4 min for the use of 24 gradient directions (25 images). However, in order to improve the SNR, data averaging was performed using magnitude images.

Partial Fourier Acquisitions

Assuming all other conditions to be constant (e.g., the spatial resolution), the SNR of a spin-warp image is proportional to the square root of the number of echo signals acquired, that is the number of lines in k-space. Accordingly, PF acquisitions decrease the SNR by the square root of the reduction factor. While this applies to EPI, it is not true for single-shot STEAM MRI. The sequence benefits from the fact that a lower number of stimulated echoes allows for a considerably higher flip angle of the readout pulses and a corresponding gain in SNR. It is noteworthy, that this improvement may be obtained without deterioration of the point-spread function (PSF) or true nominal pixel resolution of a single-shot STEAM image. In fact, if the full width of half maximum (true resolution) as obtained for FF phase encoding (1),

$$\mathrm{FWHM} = \frac{2\mathrm{FOV}}{\pi}\left(\mathrm{TR}/T_1 - \ln\cos\alpha_{\mathrm{FF}}\right), \qquad [1]$$

is maintained for HF phase encoding, then the corresponding maximum flip angle yields

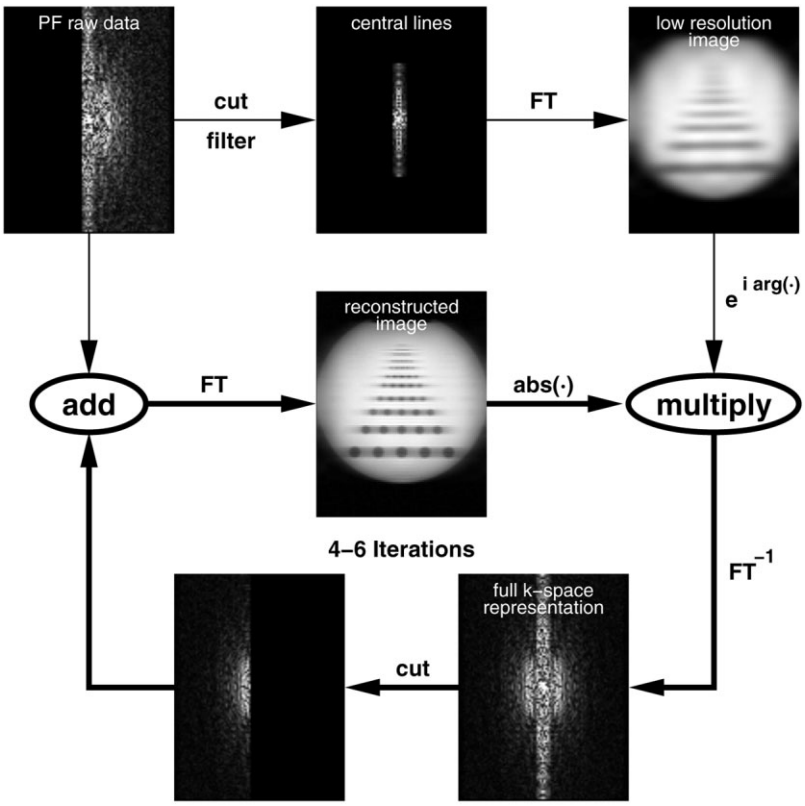

FIG. 2. Schematic diagram of the POCS algorithm. The images refer to the first approximation. Best results are obtained after four to six iterations.

$$\cos\alpha_{HF} = \cos^2(\alpha_{FF}) \cdot e^{-TR/T_1} \quad [2]$$

with $\cos\alpha_{FF}$ given by Eq. [1]. This derivation follows the ideas outlined in Ref. (2).

In the general case of PF imaging, it is advantageous to sample the n_c symmetric lines of the central k-space with centric reordering and all outer lines $l > n_c$ extending to one side of k-space with ascending order. The procedure suggests the use of two different flip angles for the inner and outer segments of k-space, which would result in a discontinuity in the decay of stimulated echoes. The problem may be avoided by introducing variable flip angles which can be recursively calculated according to

$$\tan\alpha_l = \sin\alpha_{l+1} \cdot e^{\pi FWHM/(2 \cdot FOV) - TR/T_1} \quad \text{for } l \le n_c \quad [3]$$

$$\tan\alpha_l = \sin\alpha_{l+1} \cdot e^{\pi FWHM/FOV - TR/T_1} \quad \text{for } l > n_c\,. \quad [4]$$

In contrast to the signal behavior obtained for a constant flip angle α_{HF}, variable flip angles modulate the effect on the PSF by a slightly lower start value, which then increases toward 90° for the final pulse (3).

The relative SNR (rSNR) of both approaches may be estimated from the flip angles for the central lines in k-space:

$$rSNR = SNR_{PF}/SNR_{FF} \propto \sin\alpha_{PF}/\sin\alpha_{FF} \cdot \sqrt{5/8}\,. \quad [5]$$

An even better measure of performance is the rSNR per unit time,

$$rSNR_u = rSNR/\sqrt{Acq}\,, \quad [6]$$

with Acq the image acquisition time. Depending on the actual experimental parameters, that is TR values of 7–9 ms and T_1 values of 700–800 ms, single-shot STEAM MRI with 5/8 PF encoding promises a theoretical gain of the rSNR of about 10–20%.

Image Reconstruction

A proper reconstruction of images from PF data with phase inhomogeneities requires a regeneration of the full symmetric data set in k-space. The method used here was originally proposed by Cuppen and van Est (4) and translated into the more general mathematical framework of the POCS algorithm by Liang (5). The central idea of POCS is to constrain the symmetrization process in k-space by a pre-estimated phase and to simultaneously ensure consistency with the original data. As illustrated in Fig. 2, the POCS algorithm comprises the following steps:

(i) A first approximate image $\rho_l(x)$ ($l = 0$) is reconstructed by zero filling of the original PF data and Fourier transformation.

(ii) A low-resolution phase image $\phi(x)$ is obtained from the low-frequency portion of the PF data followed by filtering (here along both the phase- and frequency-encoding dimension), zero filling, and Fourier transformation.

(iii) The reconstructed image $\rho_l(x)$ is forced to fulfill the phase constraint by setting

$$\rho'_l(x) = |\rho_l(x)| \cdot e^{i\phi(x)}\,. \quad [7]$$

(iv) Subsequently, an inverse Fourier transformation of image $\rho'_l(x)$ serves to generate a full k-space representation.

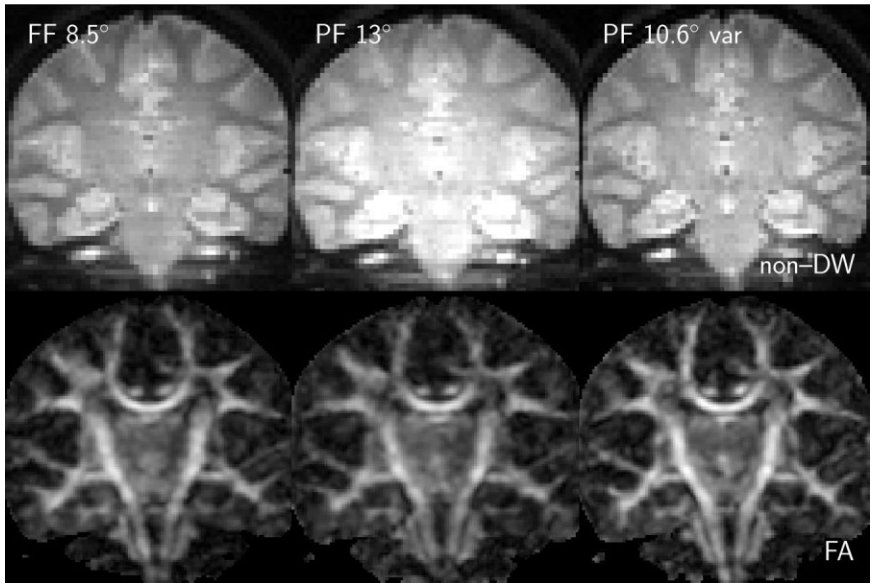

FIG. 3. (**Top**) Single-shot STEAM images ($2 \times 2 \times 4$ mm^3, raw data) without diffusion-weighting of the brain of a normal subject and (**bottom**) corresponding maps (interpolated to $1 \times 1 \times 4$ mm^3) of the fractional anisotropy (FA) obtained for FF phase encoding with a static flip angle of 8.5° as well as for 5/8 PF phase encoding with a static flip angle of 13° and a series of variable flip angles (10.6° for the central line).

(v) Where experimental *k*-space data are available, the estimated lines are replaced with the original PF acquisition. The procedure yields a new *k*-space representation which, after Fourier transformation, refers to an image $\rho_{I+1}(x)$ that is consistent with the raw data.

Upon iteration of steps (iii) to (v) the algorithm converges rapidly to an image that satisfies both the phase constraint and the data consistency. Nevertheless, the final image quality clearly depends on the quality of the true phase information obtainable from the original raw data. In order to cope with the degree of phase inhomogeneity observed in human brain in vivo, the use of only a very small number of central lines (e.g., $n_c \leq 10$) as typically acquired for HF imaging is not sufficient. For single-shot STEAM MRI as used here, 5/8 PF encoding with an acquisition matrix of 80×128 data points led to a total of 50 lines. The corresponding coverage of the central *k*-space by $n_c = 20$ lines resulted in high-quality images after only 4–6 iterations.

RESULTS AND DISCUSSION

Figure 3 shows non-DW images and corresponding fractional anisotropy (FA) maps of the human brain in vivo, which were obtained by DW single-shot STEAM MRI as outlined above. The results refer to FF phase encoding with a constant (optimized) flip angle and PF encoding with either a constant flip angle or a series of variable flip angles. Although PF encoding with constant maximum flip angle yields the highest overall signal, this achievement is at the expense of affecting the PSF and causes image blurring. Best results are obtained for PF images acquired with a variable flip angle. As demonstrated by a comparison of respective FA maps, the approach markedly improves both the spatial homogeneity of anisotropy values and the sharpness of contrast borders relative to PF images with constant flip angle. Moreover, using a region of interest covering gray and white matter, the theoretically predicted signal increase for a PF version with variable flip angle relative to FF phase encoding with constant flip angle was experimentally determined to be 16% for rSNR and 20% for $rSNR_u$.

Figure 4 depicts selected results from DTI studies of the human brain. Two different sequences were implemented at 2×2 mm^2 in-plane resolution (interpolated to 1×1 mm^2). While one version primarily aims at clinical assessments of diffusion anisotropy using 18 sections at 4-mm thickness and 12 diffusion-encoding gradient directions (together with one non-DW image), the other approach is optimized to facilitate subsequent fiber tracking using isotropic 2-mm resolution (38 sections) and 24 gradient directions (plus one non-DW image). Accordingly, the maps shown in the top row of Fig. 4 correspond to a selected 4-mm section acquired within a measuring time of 8.5 min (5 averages), while the bottom maps at 1-mm thickness were obtained from 2-mm sections acquired in 29.5 min measuring time (4 averages). In either case the maps of the main diffusion direction (MDD, Fig. 4, left) identify all major tracts crossing through this transverse section including fibers in the corpus callosum, internal and external capsule, fornix, and sagittal stratum (optic radiation) as well as arcuate fibers.

The transparent overlays of the MDD maps onto the T_1-weighted anatomy (Fig. 4, right) confirm the absence of geometric distortions due to susceptibility differences. Thus, the spatial congruence of the STEAM-derived diffusion data with anatomic MRI recordings allows for a direct correspondence without the need for a postacquisition correction method.

CONCLUSIONS

DW single-shot STEAM MRI offers considerable potential for DTI of the human brain. This particularly applies to regions that are affected by pronounced susceptibility differences. The spatial congruence of STEAM-derived diffusion maps with conventional anatomic scans seems to be a prerequisite for reliable clinical applications and is certainly beneficial for fiber tracking. Respective results will be published elsewhere.

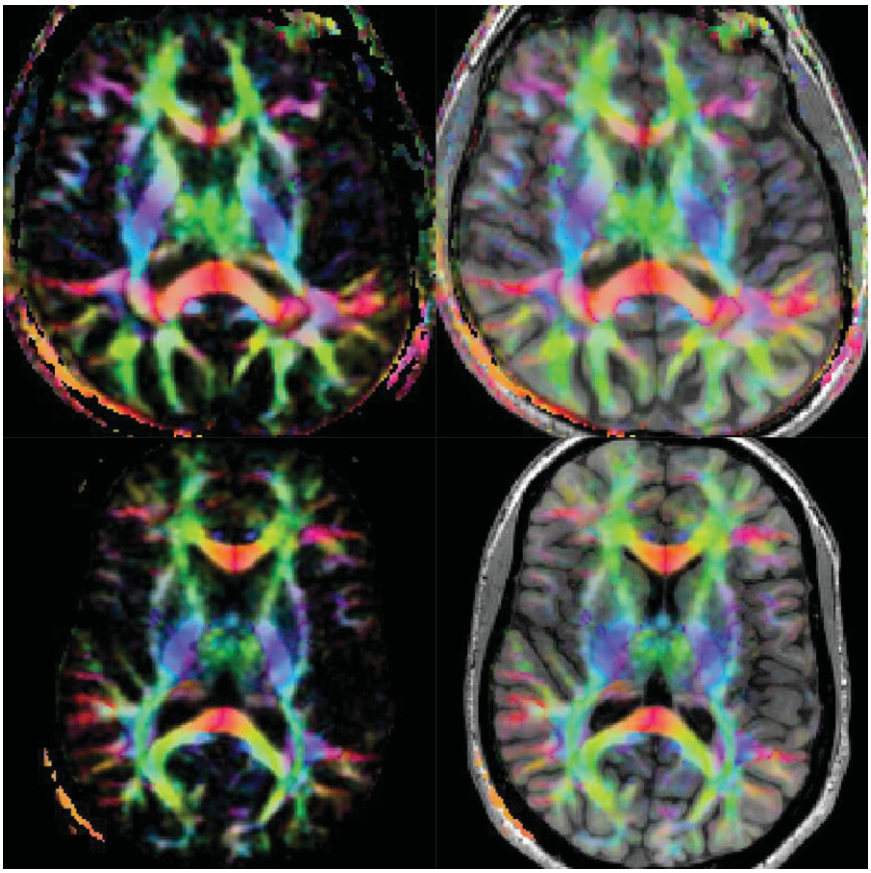

FIG. 4. DTI of the brain of normal subjects using DW single-shot STEAM MRI using 5/8 PF phase encoding with variable flip angles. (**Left**) FA-weighted MDD maps and (**right**) transparent overlays onto the corresponding T_1-weighted anatomy without the need for a coregistration algorithm. Colors refer to anatomic orientations from right to left (red), anterior to posterior (green), and dorsal to ventral (blue) or reverse. The maps represent DW images ($b = 1000$ s mm^{-2}) acquired at (top) $2 \times 2 \times 4$ mm^3 resolution (18 sections, 5 averages, measuring time 8.5 min, interpolated to $1 \times 1 \times 4$ mm^3) using 12 gradient directions, and (bottom) $2 \times 2 \times 2$ mm^3 resolution (38 sections, 4 averages, measuring time 29.5 min, interpolated to $1 \times 1 \times 1$ mm^3) using 24 gradient directions.

A decision regarding whether a particular DTI study should be based on single-shot STEAM or EPI must consider the actual question as well as the experimental boundary conditions. In the presence of susceptibility-induced signal void or geometric distortions, the STEAM DTI approach may provide a suitable solution. On the other hand, without major susceptibility problems, EPI-based DTI still benefits from a better SNR and speed. However, further technical advances are foreseeable and, apart from the use of complex data averaging methods and improved coil designs, include preliminary combinations of DW single-shot STEAM with parallel imaging (9,10).

ACKNOWLEDGMENTS

The authors thank Dr. Jürgen Finsterbusch for contributions to an earlier version of the STEAM sequence.

REFERENCES

1. Nolte UG, Finsterbusch J, Frahm J. Rapid isotropic diffusion mapping without susceptibility artifacts: whole brain studies using diffusion-weighted single-shot STEAM MR imaging. Magn Reson Med 2000;44:731–736.
2. Finsterbusch J, Frahm J. Half-Fourier single-shot STEAM MRI. Magn Reson Med 2002;47:611–615.
3. Rieseberg S. Kartierung des Diffusionstensors mittels schneller NMR-Tomografie. Axonale Konnektivität im menschlichen Gehirn. Thesis, Georg-August-Universität, Göttingen: Cuvillier-Verlag; 2004.
4. Cuppen JJ, van Est A. Reducing MR imaging time by one-sided reconstruction. Topical Conference on Fast MRI Techniques, 1987, Cleveland.
5. Liang ZP, Boada FE, Constable RT, Haacke EM, Lauterbur PC, Smith MR. Constrained reconstruction methods in MR imaging. Rev Magn Reson Med 1992;4:67–185.
6. Frahm J, Haase A, Matthaei D, Merboldt KD, Hänicke W. Rapid NMR imaging using stimulated echoes. J Magn Reson 1985;65:130–135.
7. Hasan KM, Parker DL, Alexander AL. Comparison of gradient encoding schemes for diffusion-tensor MRI. J Magn Reson Imaging 2001;13:769–780.
8. Batchelor PG, Atkinson D, Hill DLG, Calamante F, Connelly A. Anisotropic noise propagation in diffusion tensor MRI sampling schemes. Magn Reson Med 2003;49:1143–1151.
9. Finsterbusch J, Koch MA. (Almost) free lunch: Single-shot STEAM MRI with GRAPPA. In: Proceedings of the11th Annual Meeting of ISMRM, Toronto, Canada, 2003. p 1012.
10. Finsterbusch J, Koch MA. Single-shot STEAM MRI combined with SENSE. In: Proceedings of the 12th Annual Meeting of ISMRM, Kyoto, Japan, 2004. p 2251.